Volume 12
Number 21
7 June 2024
Pages 4991–5262

Journal of Materials Chemistry B

Materials for biology and medicine

rsc.li/materials-b

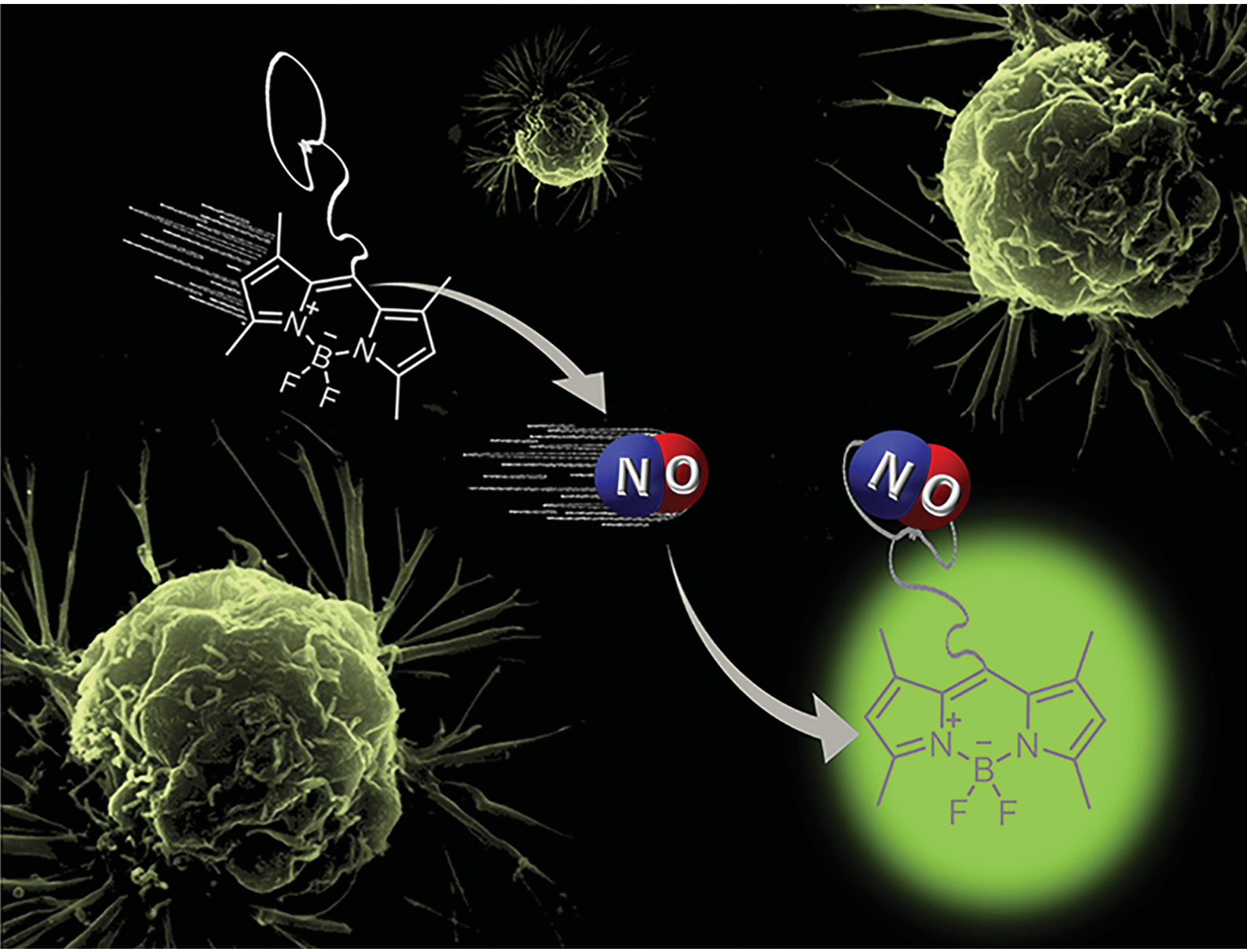

ISSN 2050-750X

ROYAL SOCIETY OF CHEMISTRY

PAPER

Salvatore Sortino *et al.*

A fluorescent probe with an ultra-rapid response to nitric oxide

Journal of Materials Chemistry B

ROYAL SOCIETY OF CHEMISTRY

PAPER

View Article Online
View Journal | View Issue

Check for updates

Cite this: J. Mater. Chem. B, 2024, 12, 5076

A fluorescent probe with an ultra-rapid response to nitric oxide†

Cristina Parisi,[a] Arianna Pastore,[b] Mariano Stornaiuolo [b] and Salvatore Sortino *[a]

Nitric oxide (NO) is a diatomic inorganic free radical ubiquitous in mammalian tissues and cells that plays a multifaceted role in a variety of physiological and pathophysiological processes. The strict dependence of the biological effects of NO on its concentration makes its real-time monitoring crucial. In view of the reactivity of NO with multiple bio-targets, the development of NO sensors that associate a fast response rate with selectivity and sensitivity is very challenging. Herein we report a fluorescent NO probe based on a BODIPY fluorogenic unit covalently linked to a trimethoxy aniline derivative through a flexible spacer. NO leads to effective nitrosation of the highly electron-rich amino active site of the probe through the secondary oxide N_2O_3, resulting in an increase of BODIPY fluorescence quantum yield from Φ_f = 0.06 to Φ_f = 0.55, accompanied by significant changes in the relative amplitude of the fluorescence lifetimes. *In situ* generation of NO, achieved by a tailored light-activatable NO releaser, allows the real-time detection of NO as a function of its concentration and permits demonstrating that the probe exhibits a very fast response time, being $\leq$0.1 s. This remarkable data combines with the high sensitivity of the probe to NO (LOD = 35 nM), responsiveness also to $ONOO^-$, the other important secondary oxide of NO, independence from the fluorescence response within a wide pH range, good selectivity towards different analytes and small interference by typical physiological concentrations of glutathione. Validation of this probe in melanoma cell lines is also reported.

Received 10th January 2024,
Accepted 20th March 2024

DOI: 10.1039/d4tb00064a

rsc.li/materials-b

Open Access Article. Published on 21 March 2024. Downloaded on 5/4/2026 9:50:04 PM.
This article is licensed under a Creative Commons Attribution 3.0 Unported Licence.

Introduction

Nitric oxide (NO) is an ubiquitous gaseous messenger with a half-life of *ca.* 5 s and diffusion radius in the range of 40–200 μm in tissues.[1] This ephemeral inorganic free radical is a pivotal bioregulator of vital functions in the human body spanning neurotransmission, hormone secretion and vasodilatation.[2] Besides, NO has proven to play a multifaceted role in bacterial infection,[3] oxidative[4] and platelet aggregation processes,[5] wound healing,[6] and neurodegenerative,[7] cardiovascular[8] and cancer diseases.[9] This wealth of properties has made NO one of the most studied molecules in the fascinating realm of biomedical sciences, not only for a better understanding of its chemico-biological mechanistic aspects but also for the exciting prospects it offers as an unconventional therapeutic in tackling severe diseases.[10] However, concentration, site of action and doses strictly dictate the outcome of NO biological effects, which, in some cases (*i.e.* cancer), can even switch from beneficial to deleterious.[11]

This scenario has pushed many efforts towards the development of sensitive and selective methodologies for NO detection. Among these, fluorescence-based approaches combine a number of peculiar advantages over other imaging techniques, such as noninvasiveness, selectivity, sensitivity, spatiotemporal resolution and easy experimental feasibility.[12–15] The last two decades have witnessed enormous progress in the development of fluorescent probes for NO detection, making it a hot topic in the crowded arena of optical sensors for bio-relevant agents. A great arsenal of the most relevant fluorescent NO probes and their related working mechanisms is illustrated and discussed in some recent review papers.[16–21] However, despite the high sensitivity and selectivity, most of the fluorescent probes developed over these years exhibit slow response to NO, which falls typically in the minutes time domain. The fast responsiveness to NO is a very important requisite for an NO sensor. In fact, the reactivity of NO (or its oxidation products) towards multiple biological targets can represent a drawback for its detection. Therefore, the development of fluorescent probes exhibiting a rapid response to NO (or its oxidation products) without precluding sensitivity and selectivity is very challenging. In this regard, some examples of fluorescent NO probes with a

[a] PhotoChemLab, Department of Drug and Health Sciences, University of Catania, I-95125, Italy. E-mail: ssortino@unict.it
[b] Department of Pharmacy, University of Napoli Federico II, Via Domenico Montesano 49, 80131, Napoli, Italy

† Electronic supplementary information (ESI) available: Syntheses and characterization procedures. See DOI: https://doi.org/10.1039/d4tb00064a

This journal is © The Royal Society of Chemistry 2024

Open Access Article. Published on 21 March 2024. Downloaded on 5/4/2026 9:50:04 PM.
This article is licensed under a Creative Commons Attribution 3.0 Unported Licence.

response time in the seconds time domain have been reported.[22–31] In particular, excellent papers from Guo's group reported a new class of NO sensors based on BODIPY fluorogenic units as reporters, closely linked to either 4-hydroxy or 4-methoxy secondary aromatic amine moieties as active recognition sites.[22,23] In these systems, the typical green fluorescence of BODIPY is effectively quenched by intramolecular photoinduced electron transfer (PET) from the nearby amino group. Under aerobic conditions, the actual strong nitrosating agent N_2O_3,[32] formed by NO oxidation,[33] nitrosates the active site, generating *N*-nitrosamines, which preclude the PET and restore the fluorescence of the BODIPY core.[22,23] In these cases, of course, nitrosation of the probe strongly dominates over the spontaneous hydrolysis of N_2O_3. Another work of the same group outlined the importance of the substituent effect in the aromatic ring of the secondary amine in tuning both the response time and the competitive reaction with glutathione (GSH),[34] a bio-substrate highly reactive to NO.[35] This was further confirmed by Song *et al.*, who developed a similar probe but with a less electron-rich secondary aromatic amine as the recognition site.[31] In this case, despite a response time of *ca.* 10 s, the presence of physiological concentrations of GSH significantly inhibited the sensitivity of the probe to N_2O_3 due to the competitive *S*-nitrosylation reaction with the biological substrate.[31]

Inspired by these interesting works, we pursued the goal of achieving an NO probe with shorter response time while maintaining high sensitivity and selectivity to NO. To this end, in this paper we have devised and synthesized the NO probe **BDT**, in which the BODIPY fluorogenic unit is covalently linked to a trimethoxy aniline derivative through a flexible spacer (Scheme 1). The rationale behind this design is as follows: (i) 3,4,5-trimethoxy secondary amine is expected to be a more reactive site for N_2O_3 than the previously reported 4-hydroxy and 4-methoxy secondary amine,[22,23] leading to the highly fluorescent **BDT-NO** (Scheme 1); (ii) the flexible spacer is expected to increase the rotational mobility of the amino active site, making it less constrained in a rigid molecular skeleton intimately connected to the BODIPY and, thus, further encouraging the nitrosation reaction; (iii) at the same time, the flexible spacer is long enough to ensure the appropriate spatial close proximity between the amino appendage and the BODIPY unit to make dynamic fluorescence quenching by PET feasible, despite the two components being not intimately connected by a covalent bond.

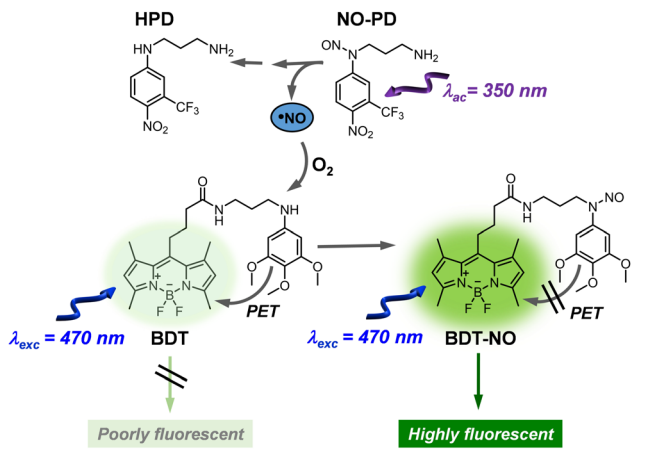

Scheme 1 Molecular structures of the NO probe **BDT**, its nitrosated product **BDT-NO**, the NO photodonor **NO-PD** and its stable photoproduct **HPD**, and the working principle.

Prompted by our long-lasting expertise in developing NO photoreleasing compounds,[36–39] in this work we decided to generate NO *in situ* by the *ad hoc* devised NO photodonor **NO-PD** (Scheme 1). Light triggering represents a unique and elegant tool for the fine regulation of the NO release process, offering a great advantage over the manual addition of different concentrations of stock solutions of NO to the probe sample. In fact, the very fast rate of photochemical reactions permits NO to be instantaneously generated (below the μs time scale) at increasing concentrations and directly in the probe compartment by the selective activation of **NO-PD** at λ_{ac} = 350 nm. Simultaneously, the evolution of the fluorescence of the probe can be monitored in real-time by its selective excitation at λ_{exc} = 470 nm as illustrated in Scheme 1.

In this work, we show that **BDT** exhibits: (i) a response time $\leq$0.1 s, much faster than that of most fluorescent NO probes developed to date; (ii) a constant fluorescence response in the pH range of 4–11, wider than that reported to date for similar BODIPY-based probes; (iii) responsiveness also to $ONOO^-$, the important NO oxidation product; and (iv) good sensitivity and selectivity towards several analytes. The suitability of the probe to detect NO photogenerated in the presence of melanoma cell lines is also demonstrated.

Results and discussion

Spectroscopic properties of BDT and BDT-NO.

Probe **BDT** and its nitrosated analogous **BDT-NO** as reference compounds were synthesized according to the procedures reported in the ESI.† Fig. 1 reports their UV-Vis absorption and fluorescence emission spectra in PBS (10 mM; pH 7.4) : MeOH 1 : 1 v/v. The intense absorption of the typical band of the BODIPY chromophore with a maximum at 497 nm is identical for both **BDT** and **BDT-NO** whereas small differences are noted in the much less intense absorption region below 350 nm, where the secondary amine and its nitrosated derivative absorb.

The identical absorption of the BODIPY chromophore for both compounds is due to the long spacer between the two functional units of the probe, which makes the BODIPY absorption feature independent of the nitrosation of the active recognition site. In contrast, the emission properties were significantly different. In fact, despite **BDT** and **BDT-NO** showing identical band profiles typical for the BODIPY fluorophore with λ_{max} = 508 nm, their quantum yields differed by almost one order of magnitude, being Φ_f = 0.06 and Φ_f = 0.55, respectively. These differences in steady-state emission were also paralleled by the fluorescence dynamic. As reported in the

Open Access Article. Published on 21 March 2024. Downloaded on 5/4/2026 9:50:04 PM.
This article is licensed under a Creative Commons Attribution 3.0 Unported Licence.

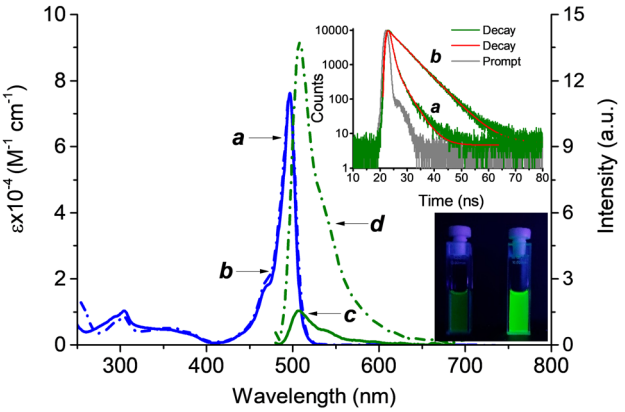

Fig. 1 Absorption spectra of **BDT** (a) and **BDT-NO** (b) and fluorescence emission spectra of optically matched solution at the excitation wavelength (λ_{exc} = 470 nm) of **BDT** (c) and **BDT-NO** (d). The photo shows the actual sample of solution c (left) and d (right) under 350 nm light. The inset shows the fluorescence decay (λ_{exc} = 455 nm, λ_{em} = 508 nm) and related bi-exponential fitting of **BDT** (a) and **BDT-NO** (b). PBS (10 mM; pH 7.4) : MeOH 1 : 1 v/v. T = 25 °C.

inset of Fig. 1, the fluorescence decay of **BDT** shows a bi-exponential behavior with a faster, dominant component having a lifetime $\tau_f \sim 0.6$ ns and relative amplitude $\alpha_f \sim 79\%$, and a slower, minor component with $\tau_s \sim 5.0$ ns and relative amplitude $\alpha_s \sim 21\%$. On the other hand, **BDT-NO** fluorescence decay showed a slower, very dominant component with $\tau_s \sim 5.2$ ns ($\alpha_s \sim 95\%$) and a minor component with $\tau_s \sim 0.60$ ns ($\alpha_s \sim 5\%$). As far as the quenched fluorescence in the case of **BDT-NO** is concerned, energy transfer between BODIPY and the trimethoxy aniline is, of course, out of question because it is highly endoergonic. As a consequence, a quenching mechanism due to PET similar to what was already proposed for BODIPY linked to secondary aromatic amine moieties, can be reasonably involved.[22,23,31] Since in our case, the fluorogenic center and the amino appendage are not intimately bound, these findings account for a dynamic-type quenching. This is in good agreement with the structural mobility of the spacer, which, as predicted, encourages the physical collision between the BODIPY fluorophore and the quencher.

Spectroscopic and photochemical properties of the NO-PD

The NO photogenerator **NO-PD** and its non-nitrosated analogous **HPD** were synthesized according to our previously reported procedures.[40] This NO photodonor was appropriately devised because its absorption spectrum falls in a spectral region where the absorption of the probe is negligible (Fig. 2A, spectrum a) and, in addition, it is non-emissive, avoiding any interference with both the absorption and fluorescence of the probe. The non-nitrosated analogous **HPD** (see Scheme 1), chosen as a model compound, exhibits similar molar absorptivity to **NO-PD** but an absorption maximum red-shifted by almost 100 nm due to the push–pull character of the nitroaniline chromophore (Fig. 2A, spectrum b).

Activation of **NO-PD** solution at λ_{ac} = 350 nm leads to the absorption spectral changes reported in Fig. 2B. They show a bleaching of the absorption band of the **NO-PD** and the formation

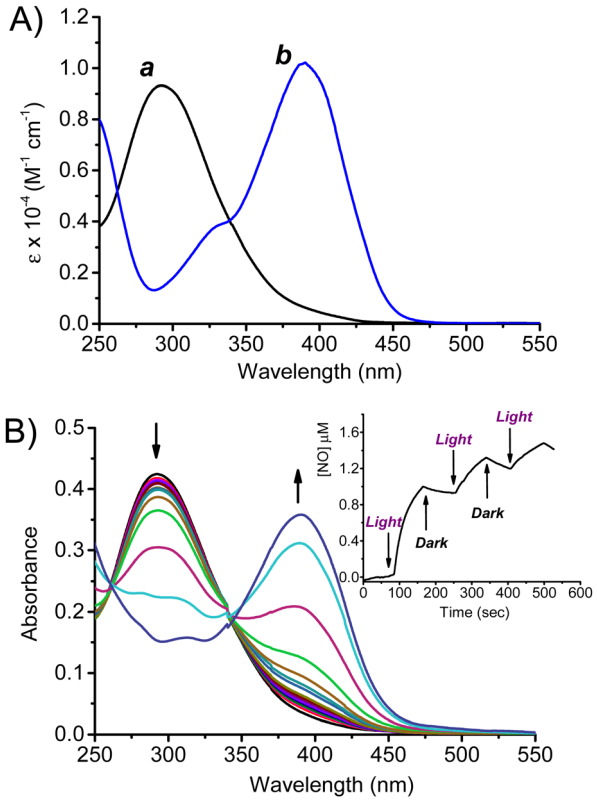

Fig. 2 (A) Absorption spectra of **NO-PD** (a) and **HPD** (b). (B) Absorption spectral changes observed upon exposure of an air-equilibrated solution of **NO-PD** (45 μM) at λ_{ac} = 350 nm for time intervals from 0 to 20 min. The arrows indicate the course of the spectral profile with the illumination time. The inset shows the NO release profile observed for a solution of **NO-PD** (45 μM) under alternate cycles of irradiation at λ_{ac} = 405 nm and dark. T = 25 °C. PBS (10 mM; pH 7.4) : MeOH 1 : 1 v/v. T = 25 °C.

of an intense absorption with a maximum at 392 nm, typical for the nitroaniline chromophore, accompanied by the presence of two isosbestic points. This photochemical profile accounts for a clean photochemical process, leading to NO release and formation of **HPD** as the only stable photoproduct, analogously to what has already been observed for other nitroso-derivatives in our previous works.[39–42] Note that photolysis is independent of the excitation wavelength, occurring with a quantum yield of $\Phi_{NO} \sim 0.03$ at $\lambda_{ac} < 420$ nm. In fact, NO release was demonstrated by its direct detection using an ultrasensitive NO electrode upon activation of **NO-PD** at λ_{ac} = 405 nm. The inset of Fig. 2B shows a prompt release of NO upon illumination that stops in the dark and restarts as the light source is turned on again.

The significant changes in the absorption spectra of **NO-PD** observed under irradiation allow the precise concentration of the generated NO to be easily calculated at any specific irradiation time by the ratio $\Delta A/\Delta\varepsilon$ where ΔA and $\Delta\varepsilon$ are the absorbance changes and the molar absorptivity at 392 nm, the wavelength where the larger differences were observed.

Properties of the BDT probe

The performances of **BDT** were evaluated by using solutions containing this probe (7 μM) and the NO photogenerator **NO-**

 This journal is © The Royal Society of Chemistry 2024

Open Access Article. Published on 21 March 2024. Downloaded on 5/4/2026 9:50:04 PM.
This article is licensed under a Creative Commons Attribution 3.0 Unported Licence.

PD (250 μM). Under these experimental conditions, the absorption spectrum of the mixture is dominated by the band of **NO-PD** in the UV region and that of **BDT** in the visible region (Fig. 3, spectrum a). This represents the ideal condition to selectively activate **NO-PD** at $\lambda_{ac} < 420$ nm for NO generation and excite **BDT** at $\lambda_{exc} > 420$ for NO detection, without reciprocal interferences. Note that the profile and absorbance of both bands are identical to those observed for the individual components at the same concentrations, ruling out any intermolecular interaction in the ground state.

Firstly, we evaluated if the NO-releasing capability of **NO-PD** was preserved in the presence of the probe. Fig. 3 shows that irradiation of the mixture with 350 nm light leads to spectral changes (spectrum b) identical to those observed for the sole **NO-PD** (see Fig. 2B for comparison), characterized by bleaching of its main absorption band accompanied by absorption at *ca.* 392 nm, typical for the stable photoproduct **HPD**. In contrast, the visible band of the BODIPY chromophore of the probe remained unaltered (Fig. 3 spectrum b). This finding confirms that **NO-PD** releases NO also in the presence of the probe, ruling out any interaction between these two components also in the excited state.

The fluorescence spectral response of the **BDT** probe to NO was therefore evaluated under the above experimental conditions. Different amounts of NO were generated by increasing the irradiation times of **NO-PD** at λ_{ac} = 350 nm in the presence of the probe. After each irradiation step, first we recorded the absorption spectrum to calculate the precise concentrations of NO produced by the increase of the absorbance at 392 nm, as described above. Thereafter (*ca.* 3 min after each irradiation step) the fluorescence spectra of the probe at λ_{exc} = 470 nm were acquired. Fig. 4A shows that the fluorescence of **BDT** significantly turns on upon increasing amounts of NO generated and reaches a limiting value after *ca.* 1 equiv. of NO (inset Fig. 4A). Note that the fluorescence spectra recorded after each irradiation step did not change over time. From the linear part of the plot reported in the inset of Fig. 4A, the limit of detection (LOD) for **BDT** is calculated to be 35 nM by using the equation LOD = $3\sigma/k$, where σ is the standard deviation of a blank measurement (n = 10) and k is the fitting of the straight line.

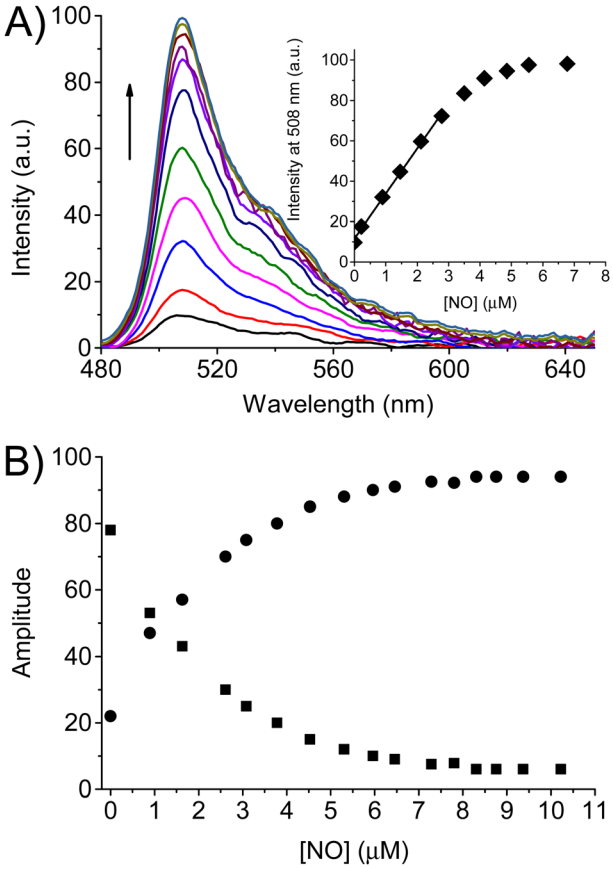

Fig. 4 (A) Fluorescence spectra of **BDT** (7 μM) observed at λ_{exc} = 470 nm upon increasing the amount of NO generated by irradiation of **NO-PD** (250 μM) with λ_{ac} = 350 nm at interval times (*s*) = 0, 25, 118, 253, 383, 543, 725, 923, 1185, 1447, and 1709, from bottom to top. The arrow indicates the course of the spectral profile with the illumination time from 0 to 28 min. The inset shows the plot of the fluorescence intensity at λ_{em} = 508 nm as a function of the NO concentration and the related linear fit. (B) Relative amplitudes of the fast (■) and slow (●) component of the fluorescence decay of **BDT** observed with increasing amount of NO generated by irradiation of **NO-PD** (250 μM) with λ_{ac} = 350 nm at different time intervals. PBS (10 mM; pH 7.4) : MeOH 1 : 1 v/v. T = 25 °C.

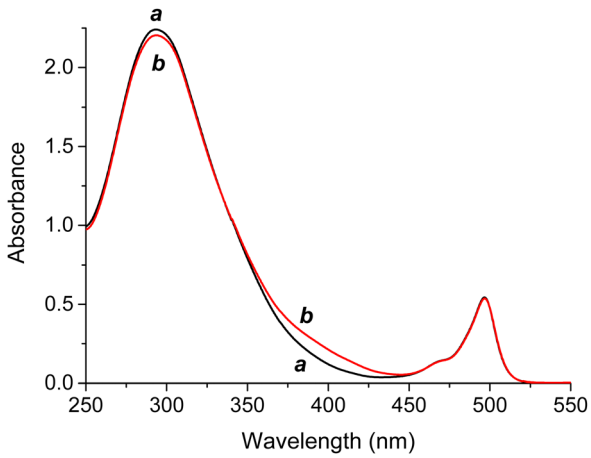

Fig. 3 Absorption spectra of a solution of **BDT** (7 μM) in the presence of **NO-PD** (250 μM) before (a) and after (b) 20 min of irradiation with 350 nm light under aerobic conditions. PBS (10 mM; pH 7.4) : MeOH 1 : 1 v/v. T = 25 °C.

The changes in steady-state emission were also well-paralleled by the behavior of the time-resolved emission. The fluorescence decay of the probe upon increasing the concentrations of NO was always bi-exponential, with lifetimes of $\tau_f \sim$ 0.60 ns and $\tau_s \sim$ 5.30 ns. However, the relative weight of these components changed dramatically and complementarily. As illustrated in Fig. 4B, the amplitude of the faster component decreased from $\alpha_f \sim$ 79% to a limiting value of $\alpha_f \sim$ 5% after the generation of *ca.* 1 equiv. of NO. An opposite effect was noted in the slower component, whose amplitude increased from $\alpha_s \sim$ 21% to limiting values $\alpha_s \sim$ 95%. The saturation values observed in both steady-state and time-resolved fluorescence are basically identical to those already reported for the

Open Access Article. Published on 21 March 2024. Downloaded on 5/4/2026 9:50:04 PM.
This article is licensed under a Creative Commons Attribution 3.0 Unported Licence.

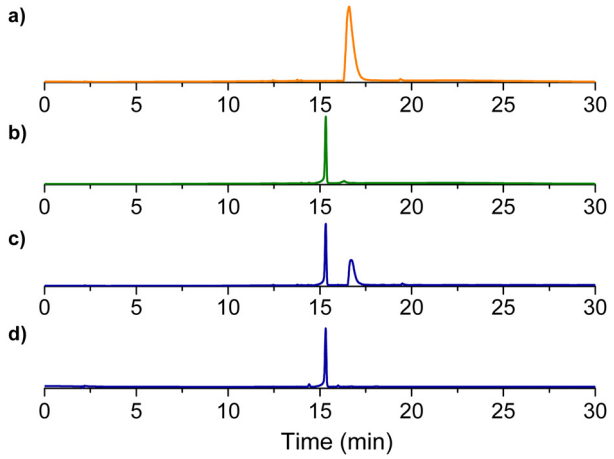

Fig. 5 A HPLC traces related to solutions of **BDT** (a), the authentic photoproduct **BDT-NO** used as a reference (b), and **BDT** after photogeneration of NO 3,5 μM f (c) and 10 μM (d). PBS (10 mM; pH 7.4) : MeOH 1 : 1 v/v. T = 25 °C.

nitrosated model compound **BDT-NO** (see Fig. 1) and provide the first indication for the formation of this product as a stable sensing product. This was well confirmed by HPLC analysis carried out with the authentic **BDT-NO** sample and the mixture **BDT** after photogeneration of different NO concentrations (Fig. 5).

The response time of **BDT** was investigated by detecting in real-time the fluorescence changes at λ_{em} = 508 nm upon its continuous excitation at λ_{exc} = 470 nm before and after turning on the continuous activation of the NO photogenerator at λ_{ac} = 350 nm. Fig. 6A (line a) shows that as the activation light is turned on, the emission intensity increases instantaneously, reaching an almost limiting value after *ca.* 1300 s. In contrast, there was no increase in the fluorescence of the control sample containing the probe **BDT** in the absence of the NO photoreleaser (line b). Interestingly, this real-time intensity increase overlaps very well with the intensity increase observed at different irradiation steps illustrated in Fig. 4A, which, for the sake of clarity, are reported as circular points in Fig. 6A. As described above, the fluorescence spectra in the experiment in Fig. 4A were acquired about 3 min after stopping the generation of NO and did not change over time. On the other hand, the integration time to acquire the fluorescence intensity in the real-time experiment shown in Fig. 6A was 0.1 s. Therefore, on the basis of the superimposed values found in the two sets of experiments, we can conclude that the nitrosation is basically complete in a time ≤0.1 s, which is much faster than the response time of several seconds exhibited by the most fluorescent probes reported to date.[22–31] What was observed was further supported by an additional real-time experiment carried out by turning ON and OFF the activation light at 350 nm while always keeping turned ON the excitation light of the probe at 470 nm. Fig. 6B clearly shows that the increase in the fluorescence intensity stops immediately as the activation light is switched OFF and no further increase in the intensity is observed with elapsing time. At this point, the

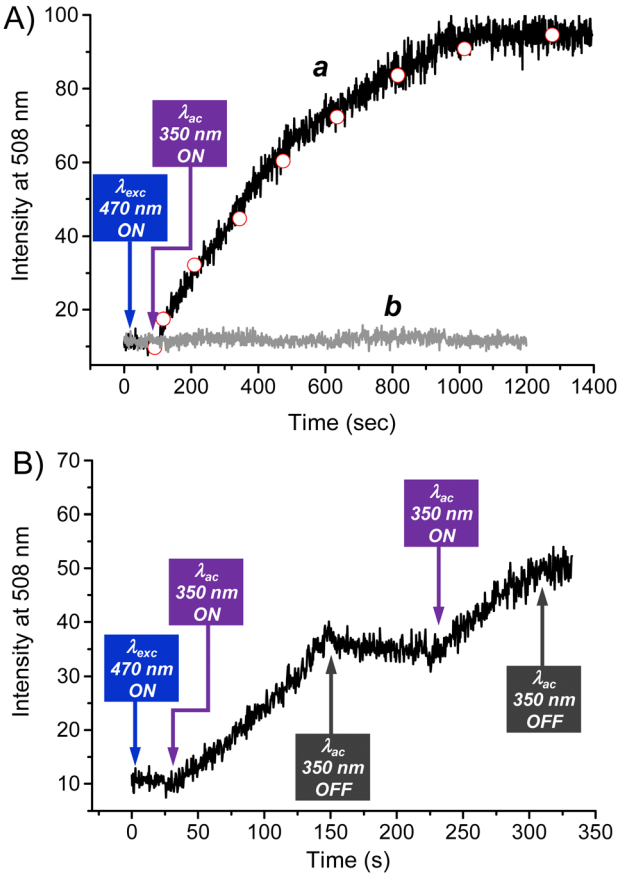

Fig. 6 (A) Real-time fluorescence intensity observed in a solution of **BDT** (7 μM) in the presence (a) and in the absence (b) of **NO-PD** (250 μM). The circles reports the fluorescence intensity as a function of the irradiation times, from 0 to 1185 s, reported in the experiment of Fig. 4A. (B) Real-time fluorescence intensity observed in a solution of **BDT** (7 μM) in the presence of **NO-PD** (250 μM) keeping constant the 470 nm excitation and alternating ON OFF cycles of the 350 nm activation light. PBS (10 mM; pH 7.4) : MeOH 1 : 1 v/v. T = 25 °C.

amount of NO photogenerated is *ca.* 0.15 equiv. As a consequence, the subsequent turning ON of the activation light results again in an increase of the fluorescence of the probe which stops and remains constant as the activation light is turned OFF. These constant values of the fluorescence intensity after stopping the NO photorelease confirm that the increase of the signal due to the highly fluorescent product **BDT-NO** is complete in a time ≤0.1 s.

To test the selectivity of the probe to NO, the response of **BDT** to several potential interfering analytes was tested. Fig. 7A shows that no significant fluorescence changes of the probe were observed, except for the peroxynitrite $ONOO^-$, for which the emission intensity reached a value basically similar to those observed for NO after the addition of only 10 μM of $ONOO^-$ (1.4 equiv.). $ONOO^-$ is the other important secondary oxide of NO and its detection with the aid of fluorescent probes is of great biological importance.[43]

The sensitivity of the probe towards $ONOO^-$ is in accordance with the well-known reactivity of this species with secondary amines *via* an electron transfer mechanism, leading to both

 This journal is © The Royal Society of Chemistry 2024

Open Access Article. Published on 21 March 2024. Downloaded on 5/4/2026 9:50:04 PM.
This article is licensed under a Creative Commons Attribution 3.0 Unported Licence.

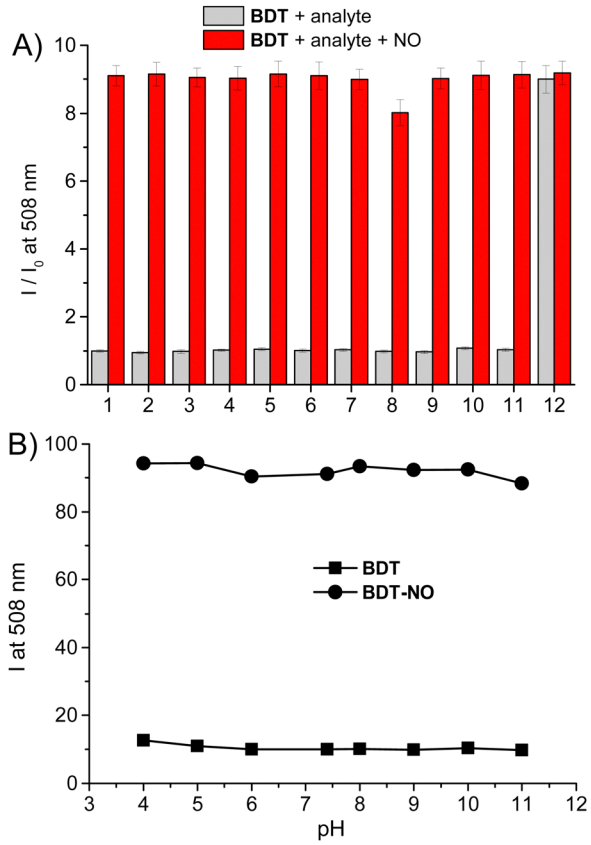

Fig. 7 (A) Fluorescence intensity ratio (λ_{exc} = 470 nm, λ_{em} = 508 nm) observed in a solution of **BDT** (7 μM) in the presence of various biologically relevant species. I and I_0 are the fluorescence intensity observed after and before the addition of the analytes (grey bars) and the analytes with subsequent generation of 70 μM NO (red bars) through the precursor **NO-PD** (250 μM), respectively. PBS (10 mM; pH 7.4) : MeOH 1 : 1 v/v. T = 25 °C. Analytes: (1) control, (2) Fe^{2+}, (3) Ca^{2+}, (4) Zn^{2+}, (5) K^+, (6) Mg^{2+}, (7) Cu^{2+}, (8) GSH, (9) H_2O_2, (10) $^{\bullet}OH$; (11) ClO^-; and (12) $ONOO^-$; concentrations of analytes: (2–8) = 1 mM; (9–11) = 100 μM; (12) = 10 μM. (B) Dependence of the fluorescence intensity (λ_{exc} = 470 nm, λ_{em} = 508 nm) of 7 μM solutions of **BDT** (■) and **BDT-NO** (●). PBS (10 mM, pH 7.4):MeOH 1 : 1 v/v. T = 25 °C.

nitroso and nitro-derivatives, with the former present in larger amounts.[44] Besides, our finding is in excellent agreement to what was recently reported by Guo *et al.* for their BODIPY-based sensor bearing a 4-methoxy-substituted secondary amine-derivative as recognition site.[23] Note that, the responsiveness to $ONOO^-$ associated with that to N_2O_3 is not a drawback in terms of selectivity but represents an additional advantage for any fluorescent NO probe and is a very challenging task. In fact, when produced intracellularly, NO could promptly react with the endogenous superoxide anion $O_2^{\bullet -}$ leading to $ONOO^-$. Since this reaction occurs at a diffusion-controlled rate (*ca.* 10^{10} M^{-1} s^{-1}),[45] it highly competes with the oxidation process of NO by molecular oxygen, resulting in a consequent reduction of the amount of N_2O_3 and the related failure of all the NO probes exclusively sensitive to N_2O_3 such as the typical *o*-diamine-type fluorescent probes.[16–21] The data reported in Fig. 7A also demonstrate that the coexistence of the same analytes as competitive species does not significantly affect the response of the **BDT** probe. Even in the presence of GSH, a bio-substrate highly sensitive to nitrosation,[35] the probe exhibited good sensitivity to NO. This is probably the result of the highly electron-rich trimethoxy aniline active site. Similar independence from the NO response in the presence of GSH was in fact reported by Guo *et al.* for fluorescent probes integrating *p*-hydroxyl and *p*-methoxy substituted secondary aromatic amine as active sites.[22,23] In contrast, the inhibitory effects of GSH on the fluorescent probe with a less electron-rich active site were reported and deeply investigated by Song and coworkers.[31]

Another interesting property of **BDT** and its sensing product **BDT-NO** is that, unlike many of the existing fluorescent probes, their emission is independent of pH over a large range of 4–11 (Fig. 7B). This represents a great advantage in light of different pH values that different cell types or different cellular compartments may have.

The suitability of **BDT** as an *in vitro* NO probe was finally tested in a cellular environment by *ad hoc* designed bio-imaging experiments using confocal fluorescence microscopy. To this end, B16 melanoma cell lines were incubated for 4 h with a solution containing both the probe **BDT** and the NO photodonor **NO-PD** and, as a control, solutions of the individual functional components and the solvent vehicle. The response time of **BDT** was investigated by detecting the real-time fluorescence changes in the green channel (λ_{em} = 508 nm) upon continuous excitation at λ_{exc} = 470 nm, before and after turning on the activation of the NO photodonor with continuous pulses (10 ms) at λ_{ac} = 405 nm, a wavelength also able to trigger NO release (see inset Fig. 2B). Fig. 8 (top panel) shows a constant, low value of the emission intensity in all samples before the activation light is switched ON. The turning ON of 405 nm light sources leads to a significant and then gradual increase in the green emission intensity in the cells incubated with both the probe and the NO photodonor (line a). On the other hand, negligible changes were observed in the control samples under identical experimental conditions (lines b,c,d). Fig. 8 (bottom) also shows representative fluorescence images taken before and after the irradiation cycle to generate NO, which further demonstrates the validity of the probe to detect this species intracellularly. The probe appears mostly localized in the cytosol of the cells. We could not detect signal enrichment at the cell membrane or in any intracellular organelles of the secretory pathway or in mitochondria. This cytosolic localization was expected since the probe does not contain moieties useful for its specific targeting in subregions of human cells.

Conclusions

We have reported the design, synthesis and properties of a new fluorescent probe for NO detection under aerobic conditions. The presence of the trimethoxy substituent in the active recognition site makes the secondary amine highly electron-rich and more reactive towards nitrosation by N_2O_3, which is complete

Open Access Article. Published on 21 March 2024. Downloaded on 5/4/2026 9:50:04 PM. This article is licensed under a Creative Commons Attribution 3.0 Unported Licence.

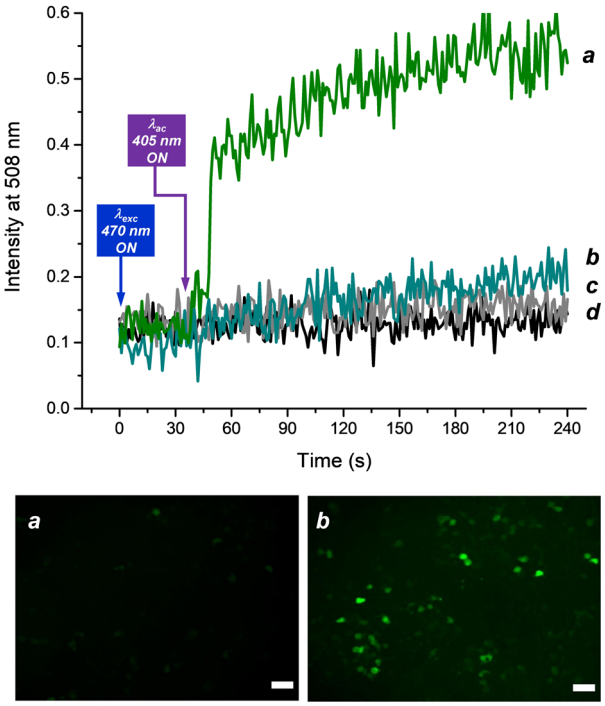

Fig. 8 (Top panel) Evolution of the green fluorescence (λ_{exc} = 470 nm) in B16 melanoma cells incubated with solutions of both **BDT** and **NO-PD** (a) **BDT** (b), **NO-PD** (c) and the solvent vehicle (d) before and after continuous pulsed activation λ_{ac} = 405 nm. (Bottom panel) Representative fluorescence images taken before (a) and after (b) the activation cycle to generate NO. [**BDT**] = 5 μM, [**NO-PD**] = 100 μM. Bare scale = 75 μm.

after the addition of *ca.* 1 equiv. of NO, turning on the emission of the BODIPY unit, originally quenched by PET. Through the photochemical NO generation achieved by an *ad hoc* used NO photodonor, we have demonstrated that the probe displays a response time in the sub-second time regime ($\leq$0.1 s). In this regard, **BDT** is superior by more than two orders of magnitude to most of the existing fluorescent NO probes. Another remarkable point of this probe is its responsiveness to $ONOO^-$, the other important secondary oxide of NO. To date, only a few probes have been reported to possess the unique ability to respond simultaneously to N_2O_3 and $ONOO^-$.[23] NO detection and imaging were successfully demonstrated by the visualization of NO photogenerated intracellularly and dependence of the emission on the NO concentration in melanoma cell lines. All the above properties, combined with the good sensitivity (LOD = 35 nM), selectivity towards several biologically relevant species, working efficiency in the presence of GSH and independence from the fluorescence response within a wide pH range, make **BDT** an intriguing candidate for further chemical and biomedical studies involving NO.

Experimental section

Chemicals

BDT and **BDT-NO**, were synthesized according to the procedures reported in the ESI.† **NO-PD** and **HPD** were synthesized according to our previously reported procedures.[40] All other chemicals were purchased by Sigma Aldrich and used as received. MilliQ water was used for the preparation of the buffer solution. All other solvents used were spectrophotometry grade.

Cell lines and fluorescence imaging at equilibrium

Melanoma (B16) cell lines were obtained from the American Type Culture Collection (ATCC, Manassas, VA, USA). Cells were cultured in Dulbecco's modified Eagle's medium with high-glucose and L-glutamine (DMEM, Lonza, Walkersville, MD, USA) in the presence of 10% fetal bovine serum (FBS), 100 U mL^{-1} penicillin and 100 μg mL^{-1} streptomycin (all from Sigma Aldrich, Milan, Italy). The standard cell culture conditions (37 °C, 95% rel. humidity, 5% CO_2) were maintained by using an incubator (Heracell 150, Thermo Scientific, Waltham, MA, USA). The indicated cells were treated with [**BDT**] = 5 μM, and/or [**NO-PD**] = 100 μM for 4 hours. After incubation, the culture medium was removed, and cells were incubated with Red Phenol free Hanks' Balanced Salt Solution at 37 °C in the dark before fluorescence investigation. A confocal laser scanning microscope (Zeiss LSM 700) equipped with stable solid-state lasers (405/444 and 488 nm) and a 40×/1.2 NA objective was used to generate a 10 second flash of blue light λ_{ac} = 405 nm to induce intracellular NO release from **NO-PD**. Intracellular **BDT** fluorescence (laser of 488 nm, exc filter 495 (450–517) nm and emission filter 519 (497–575) nm) was visualized in the cell before and after blue-light flashing.

Instrumentation

^{1}H-NMR and ^{13}C-NMR spectra were recorded on a Varian UNITY Inova at 500 MHz. Chemical shifts (δ) are given in parts per million (ppm) and the coupling constants (J) are given in Hz. The following abbreviations are used to designate peak multiplicity: s = singlet, d = doublet, dd = doublet of doublets, t = triplet, td = triplet of doublets, and m = multiplet.

Flash column chromatography was performed on silica gel (Merck Kieselgel 60, 230–400 mesh ASTM). The progress of the reactions was followed by thin layer chromatography (TLC) on 5 × 20 cm plates with a layer thickness of 0.2 mm. ESI† mass spectra were acquired on an API 2000-ABSciex using CH_3OH (negative ion mode).

The reverse-phase HPLC analyses were performed on a HP Agilent 1100 chromatograph system equipped with a binary pump (G1312A), a membrane degasser and a diode-array detector (DAD) (G1315A) integrated into the HP1100 system. Data analysis were processed using a HP ChemStation system (Agilent Technologies). The analytical column was a SUPELCOSIL C-18 (15 cm × 4, 6 mm × 5 μm). The mobile phase consisting of acetonitrile (A)/water (B), in the gradient mode (2% A/98% B at 0 min, from 2 to 100% A between 0 and 20 min and from 100 to 2% A between 20 and 30 min) at a flow-rate of 1 mL min^{-1}. The injection volume was 20 μL. The column effluent was monitored at 497 nm referenced against 700 nm wavelength.

UV-Vis spectra absorption and fluorescence emission spectra were recorded with a PerkinElmer spectrophotometer (mod. Lambda 365) and a Spex Fluorolog-2 (mod. F-111)

 This journal is © The Royal Society of Chemistry 2024

Open Access Article. Published on 21 March 2024. Downloaded on 5/4/2026 9:50:04 PM. This article is licensed under a Creative Commons Attribution 3.0 Unported Licence.

spectrofluorimeter, respectively, using quartz cells with a path length of 1 cm. Fluorescence lifetimes were recorded with the same fluorimeter equipped with a TCSPC Triple Illuminator. The samples were irradiated using a pulsed diode excitation source Nanoled at 455 nm. The kinetics were monitored at 508 nm and the solvent itself was used to register the prompt at 455 nm. The system allowed the measurement of fluorescence lifetimes from 200 ps. The exponential fit of the fluorescence decay was obtained using eqn (1):

$$I(t) = \Sigma\alpha_i \exp(^{-t/\tau i}) \quad (1)$$

where τ is the lifetime and α is the amplitude of the related component.

Direct monitoring of NO release from **NO-PD** was performed by amperometric detection with a World Precision Instrument, ISO-NO meter, equipped with a data acquisition system, and based on direct amperometric detection of NO with a short response time (<5 s) and a sensitivity range of 1 nM–20 μM. The analog signal was digitalized with a four-channel recording system and transferred to a PC. The sensor was accurately calibrated by mixing standard solutions of $NaNO_2$ with 0.1 M H_2SO_4 and 0.1 M KI according to reaction (2):

$$4H^+ + 2I^- + 2NO_2^- \rightarrow 2H_2O + 2NO + I_2 \quad (2)$$

Irradiation was performed in a thermostated quartz cell (1 cm path length, 3 mL capacity) using a continuum laser with λ_{exc} = 405 nm. NO measurements were carried out under stirring with the electrode positioned outside the light path in order to avoid NO signal artifacts due to photoelectric interference on the ISO-NO electrode.

In all other experiments, NO was generated by the activation of **NO-PD** solutions in thermostated quartz cells (1 cm path length, 3 mL capacity) under gentle stirring, using a black light phosphor lamp at λ_{ac} = 350 nm. NO photogeneration quantum yield (Φ_{NO}) was determined within the 20% transformation of **NO-PD** by using eqn (3):

$$\Phi_{NO} = [tr\text{-}\mathbf{NO\text{-}PD}]V/t(1-10^{-A}) \quad (3)$$

where [*tr*-**NO-PD**] is the concentration of phototransformed NO photodonor, V is the volume of the irradiated sample, t is the irradiation time, A is the absorbance of the sample at the excitation wavelength and I is the intensity of the excitation light source. The concentration of the phototransformed NO photodonor was determined spectrophotometrically, by taking into account the absorption changes at 392 nm and the related $\Delta\varepsilon$ at the same wavelength. I was calculated by potassium ferrioxalate actinometry.

Preparation of the samples

All sample solutions were prepared in PBS (10 mM; pH 7.4) : MeOH 1 : 1, v/v under air-equilibrated conditions at 25 °C. The concentration of NO generated was calculated by monitoring the absorption increase at 392 nm after each irradiation time and using a $\Delta\varepsilon$ = 9000 M^{-1} cm^{-1} at the same wavelength. A stock solution of the probe was prepared in MeOH and then appropriately diluted with PBS to obtain a final concentration of 7.0 μM.

The aqueous solutions of K^+, Ca^{2+}, Mg^{2+}, Zn^{2+}, Fe^{2+} and Cu^{2+} were freshly prepared from their chloride salts. An aqueous solution of GSH (10 mM) was freshly prepared. $HO^\bullet$ was generated *in situ* by the Fenton reaction, and its concentration was equal to the Fe^{2+} concentration. $FeSO_4$ was used for the Fenton reaction. H_2O_2 solution was prepared by dilution of commercial H_2O_2 solution in deionized water, and its concentration was determined by using an extinction coefficient of 43.6 M^{-1} cm^{-1} at 240 nm. ClO^- solution was prepared by dilution of commercial NaClO solution in deionized water, and its concentration was determined using an extinction coefficient of 350 M^{-1} cm^{-1} at 292 nm. $ONOO^-$ was photochemically generated from a photoprecursor (20 μM) activatable by red light, previously developed in our group and possessing spectroscopic features not interfering with the probe.[39] Various analytes, except $HO^\bullet$, were directly added to the solution of the sensor and after 15 minutes of incubation (15 min of irradiation for the $ONOO^-$ photoprecursor) the fluorescence spectra were recorded. In the case of $HO^\bullet$, the probe and H_2O_2 were premixed, and then Fe^{2+} was added to the mixture. In the case of competitive experiments with the analytes, NO was photogenerated after the same incubation time as reported above.

Time resolved fluorescence live cell imaging

Time-resolved fluorescence assays were performed using an EnVision™ multimode Plate Reader (PerkinElmer 2105). Murine B16 cells were plated in a black 96-well Optiplate (PerkinElmer) (5.000 cells per well). 16 hours after seeding, the cells were treated with [**BDT**] = 5 μM, and/or [**NO-PD**] = 100 μM for 4 hours. After incubation, the culture medium was replenished with Red Phenol free Hanks' Balanced Salt Solution (50 μL per well) and cells were incubated at 37 °C in the EnVision instrument in the dark. Fluorescence readings were taken in a continuous mode with time intervals of 1 s. A continuous series of 10 ms flashes at λ_{ac} = 405 nm was used to induce intracellular NO release from **NO-PD**. λ_{exc} = 470 nm and λ_{em} = 508 nm were used to monitor **BDT** fluorescence. The instrument settings for fluorescence measurements included the use of a monochromator installed in the instrument. The detector was set to an eight of 6.5 mm. Excitation light power and detector gain were set at 100% and 750 respectively.

Conflicts of interest

There are conflicts to declare.

Acknowledgements

This research was funded by the European Union - NextGenerationEU through the Italian Ministry of University and Research under PNRR - M4C2-I1.3 Project PE_00000019 "HEAL ITALIA and by PNRR-M4C2- I1.1 – MUR Call for proposals n.

1409 of 14-09-2022 - PRIN 2022 PNRR - ERC sector PE4- Project title: A molecular platform for intracellular nitric oxide sensing - Project Code P2022F4WR8- CUP Code D53D23016840001- Funded by the European Union – NextGenerationEU

Open Access Article. Published on 21 March 2024. Downloaded on 5/4/2026 9:50:04 PM. This article is licensed under a Creative Commons Attribution 3.0 Unported Licence.

Notes and references

1 L. J. Ignarro, *Nitric Oxide: Biology and Pathobiology*, Elsevier Inc., 2nd edn, 2010.
2 L. J. Ignarro, *Arch. Pharmacal. Res.*, 2009, **32**, 1099–1101.
3 L. Yang, E. S. Feura, M. J. R. Ahonen and M. H. Schoenfisch, *Adv. Healthcare Mater.*, 2018, **7**, 1–18.
4 L. Packer, *Methods in Enzymology, Nitric Oxide, Part C: Biological and Antioxidant Activities*, Academic Press, San Diego, 1999, 301.
5 G. Walford and J. Loscalzo, *J. Thromb. Haemostasis*, 2003, **1**, 2112–2118.
6 M. J. Malone-Povolny, S. E. Maloney and M. H. Schoenfisch, *Adv. Healthcare Mater.*, 2019, **8**, 1–18.
7 D. Tewari, A. N. Sah, S. Bawari, S. F. Nabavi, A. R. Dehpour, S. Shirooie, N. Braidy, B. L. Fiebich, R. A. Vacca and S. M. Nabavi, *Curr. Neuropharmacol.*, 2021, **19**, 114–126.
8 C. Farah, L. Y. M. Michel and J. L. Balligand, *Nat. Rev. Cardiol.*, 2018, **15**, 292–316.
9 D. Fukumura, S. Kashiwagi and R. K. Jain, *Nat. Rev. Cancer*, 2006, **6**, 521–534.
10 A. W. Carpenter and M. H. Schoenfisch, *Chem. Soc. Rev.*, 2012, **41**, 3742–3752.
11 Z. Huang, J. Fu and Y. Zhang, *J. Med. Chem.*, 2017, **60**, 7617–7635.
12 J. F. Woolley, J. Stanicka and T. G. Cotter, *Trends Biochem. Sci.*, 2013, **38**, 556–565.
13 Z. J. Tonzetich, L. E. McQuade and S. Lippard, *J. Inorg. Chem.*, 2010, **49**, 6338–6348.
14 T. Nagano, *J. Clin. Biochem. Nutr.*, 2009, **45**, 111–124.
15 L. E. McQuade and S. J. Lippard, *Curr. Opin. Chem. Biol.*, 2010, **14**, 43–49.
16 B. Almeida, K. E. Rogers, O. K. Nag and J. B. Delehanty, *ACS Sens.*, 2021, **6**, 1695–1703.
17 Y. Chen, *Nitric oxide*, 2020, **98**, 1–19.
18 M. Yang, J. Fan, J. Du and X. Peng, *Chem. Sci.*, 2020, **11**, 5127–5141.
19 X. Chen, F. Wang, J. Y. Hyun, T. Wei, J. Qiang, X. Ren, I. Shin and J. Yoon, *Chem. Soc. Rev.*, 2016, **45**, 2976–3016.
20 Z. Xu and L. Xu, *Chem. Commun.*, 2016, **52**, 1094–1119.
21 H. Li and A. Wan, *Analyst*, 2015, **140**, 7129–7141.
22 J. Miao, Y. Huo, X. Lv, Z. Li, H. Cao, H. Shi, Y. Shi and W. Guo, *Biomaterials*, 2016, **78**, 11–19.
23 Y. Huo, J. Miao, J. Fang, H. Shi, J. Wang and W. Guo, *Chem. Sci.*, 2019, **10**, 145–152.
24 Y. Huo, J. Miao, L. Han, Y. Li, Z. Li, Y. Shi and W. Guo, *Chem. Sci.*, 2017, **8**, 6857–6864.
25 Y. Huo, J. Miao, Y. Li, Y. Shi, H. Shi and W. Guo, *J. Mater. Chem. B*, 2017, **5**, 2483–2490.
26 C. G. Dai, J. L. Wang, Y. L. Fu, H. P. Zhou and Q. H. Song, *Anal. Chem.*, 2017, **89**, 10511–10519.
27 P. Rogelio Escamilla, Y. Shen, Q. Zhang, D. S. Hernandez, C. J. Howard, X. Qian, D. Y. Filonov, A. V. Kinev, J. B. Shear, E. V. Anslyn and Y. Yang, *Chem. Sci.*, 2020, **11**, 1394–1403.
28 Y. Yang, S. K. Seidlits, M. M. Adams, V. M. Lynch, C. E. Schmidt, E. V. Anslyn and J. B. Shear, *J. Am. Chem. Soc.*, 2010, **132**, 13114–13116.
29 C. B. Huang, J. Huang and L. Xu, *RSC Adv.*, 2015, **5**, 13307–13310.
30 C. Li, W. J. Tang, W. Feng, C. Liu and Q. H. Song, *Anal. Chim. Acta*, 2020, **1096**, 148–158.
31 H. Li, Y. H. Hao, W. Feng and Q. H. Song, *J. Mater. Chem. B*, 2020, **8**, 9785–9793.
32 T. A. Heinric, R. S. da Silva, K. M. Miranda, C. H. Switzer, D. A. Wink and J. M. Fukuto, *Br. J. Pharmacol.*, 2013, **169**, 1417–1429.
33 D. A. Wink, J. F. Darbyshire, R. W. Nims, J. E. Saavedra and P. C. Ford, *Chem. Res. Toxicol.*, 1993, **6**, 23–27.
34 Q. Xue, S. Wang, X. Bi, Z. Chen, H. Zhu, W. Chen, H. Lu and Z. Guo, *Dyes Pigm.*, 2023, **218**, 111486.
35 D. A. Wink, R. W. Nims, J. F. Derbyshire, D. Christodoulou, I. Hanbauer, G. W. Cox, F. Laval, J. Laval, J. A. Cook, M. C. Krishna, W. G. DeGraff and J. B. Mitchell, *Chem. Res. Toxicol.*, 1994, **7**, 519–525.
36 S. Sortino, *Chem. Soc. Rev.*, 2010, **39**, 2903–2913.
37 E. B. Caruso, S. Petralia, S. Conoci, S. Giuffrida and S. Sortino, *J. Am. Chem. Soc.*, 2007, **129**, 480–481.
38 A. Fraix, C. Parisi, M. Seggio and S. Sortino, *Chem. – Eur. J.*, 2021, **27**, 12714–12725.
39 C. Parisi, M. Failla, A. Fraix, L. Menilli, F. Moret, E. Reddi, B. Rolando, F. Spyrakis, L. Lazzarato, R. Fruttero, A. Gasco and S. Sortino, *Chem. Sci.*, 2021, **12**, 4740–4746.
40 C. Parisi, M. Failla, A. Fraix, B. Rolando, E. Gianquinto, F. Spyrakis, E. Gazzano, C. Riganti, L. Lazzarato, R. Fruttero, A. Gasco and S. Sortino, *Chem. – Eur. J.*, 2019, **25**, 11080–11084.
41 A. Fraix, C. Parisi, M. Failla, K. Chegaev, F. Spyrakis, L. Lazzarato, R. Fruttero, A. Gasco and S. Sortino, *Chem. Commun.*, 2020, **56**, 6332–6335.
42 C. Parisi, A. Fraix, S. Guglielmo, F. Spyrakis, B. Rolando, L. Lazzarato, R. Fruttero, A. Gasco and S. Sortino, *Chem. – Eur. J.*, 2020, **26**, 13627–13633.
43 L. Wu, Y. Wang, M. Weber, L. Liu, A. C. Sedgwick, S. D. Bull, C. Huang and T. D. James, *Chem. Commun.*, 2018, **54**, 9953–9956.
44 M. Masuda, H. F. Mower, B. Pignatelli, I. Celan, M. D. Friesen, H. Nishino and H. Ohshima, *Chem. Res. Toxicol.*, 2000, **13**, 301–308.
45 S. Goldstein and G. Czapski, *Free Radical Biol. Med.*, 1995, **19**, 505–510.

 This journal is © The Royal Society of Chemistry 2024